The Role of Compositional Tuning on Thermoelectric Parameters of Hybrid Halide Perovskites

*Md Azimul Haque, Mohamad Insan Nugraha, Sri Harish Kumar Paleti, Derya Baran**

King Abdullah University of Science and Technology (KAUST), Physical Science and Engineering Division (PSE), KAUST Solar Center (KSC), Thuwal 23955-6900, Saudi Arabia

*E-mail: derya.baran@kaust.edu.sa

ABSTRACT: Halide perovskites are emerging as a new class of materials for thermoelectric applications owing to their low thermal conductivity and high seebeck coefficient (thermopower). In this work, the thermoelectric parameters of vapor deposited hybrid perovskite thin films are explored for the first time. We establish a relationship between the chemical composition and thermoelectric properties of sequentially vapor deposited $CH_3NH_3PbI_3$ films. A composition dependent grain size and in-plane electrical conductivity evolution is observed and its influence on thermoelectric properties is analyzed. An ultralow in-plane thermal conductivity of 0.32 ± 0.03 $Wm^{-1}K^{-1}$ at room temperature is recorded for $CH_3NH_3PbI_3$ using a chip-based 3ω method. Thermal conductivity measurement of a series of $CH_3NH_3PbI_3$ films reveal that the thermal transport is governed by Pb-I lattice at room temperature. Furthermore, n- and p-type $CH_3NH_3PbI_3$ films achieved by compositional tuning exhibit high negative (6500 µV/K) and positive (5500 µV/K) thermopower.

1. INTRODUCTION

Hybrid halide perovskites have recently received exponential interest due to their extraordinary photovoltaic performances.[1-5] Apart from solar cells, multitude of other applications such as photodetectors, lasers, LEDs, and memory devices have been already demonstrated underpinning the versatile nature of halide perovskites.[6-9] Hybrid halide perovskites with the general formula $CH_3NH_3MX_3$, where M= Sn, Pb and X= Cl, Br, I, have been investigated for solar cells and photodetectors, with methylammonium lead iodide ($CH_3NH_3PbI_3$) and its mixed variants ($CH_3NH_3PbI_{3-x}Cl_x$) being the most pursued perovskites.[10-13] Direct bandgap, high charge-carrier mobility, long carrier diffusion length and large light absorption coefficient coupled with facile synthesis and cost effectiveness makes hybrid perovskites suitable candidate for next generation optoelectronics.[14-16]

Despite the unprecedented performance of hybrid perovskites, their crucial physical properties such as thermal transport have received limited attention so far. The first thermal conductivity (κ) measurement on $CH_3NH_3PbI_3$ was reported by Pisoni et al. with an ultralow value of 0.5 $Wm^{-1}K^{-1}$ and 0.3 $Wm^{-1}K^{-1}$ for single crystal and polycrystalline samples, respectively at room temperature.[17] Several techniques such as steady state bar method, laser flash method, scanning near-field thermal microscopy, and time-domain thermo-reflectance along with theoretical prediction concord the ultralow thermal conductivity of hybrid perovskites with values less than 1 $Wm^{-1}K^{-1}$.[17-21] In addition, thermopower which is another important thermal property has been reported to be high (in the range 1000-5000 μV/K) for hybrid perovskite single crystals.[22,23] Ultralow thermal conductivity, high thermopower in conjunction with high carrier mobility makes hybrid perovskites a fitting candidate for future thermoelectrics. The majority of the prior work on thermal transport of hybrid perovskites is accomplished using

single crystals or polycrystalline pellets with limited information on thermopower. Furthermore, in-plane thermal conductivity and thermopower of $CH_3NH_3PbI_3$ films remain largely unexplored. The organic and inorganic component in hybrid perovskites offers the flexibility of tuning the composition and in turn, the intrinsic defects.[24] By manipulating the organic/inorganic component during growth, the intrinsic point defects responsible for self-doping in hybrid perovskites can be controlled which presents an unique possibility of tuning the electronic conductivity type (*n* or *p*).[25] Up till now, compositionally-tuned hybrid perovskites have been explored only in context to performance of solar cells.[26,27] Recently, high-quality perovskite *p*-*n* homojunctions have been realized controlling the growth conditions.[28,29] Such composition governed self-doping in hybrid perovskites can bring unexpected ramifications in its electronic and thermal behavior beneficial for thermoelectrics. While the electrical conductivity of hybrid perovskites is low compared to traditional thermoelectric materials, it is imperative to understand the intrinsic thermoelectric properties to design strategies for improvement.

In this contribution, we have grown compositionally-tuned $CH_3NH_3PbI_3$ films by controlling the conversion time of evaporated PbI_2 under CH_3NH_3I (MAI) vapor leading to MAI rich and deficient films. The influence of composition on microstructure, charge transport and thermal properties is analyzed. Measuring a series of MAI rich and deficient $CH_3NH_3PbI_3$ films indicates the in-plane thermal conductivity of $CH_3NH_3PbI_3$ is governed by the Pb-I lattice at room and higher temperatures (293-373 K). Furthermore, high negative (6500 μV/K) and positive (5500 μV/K) thermopower were obtained for the first time by tuning the composition of $CH_3NH_3PbI_3$, achieving *n*- and *p*-type films.

2. METHODS

MAI was purchased from Dyesol and PbI_2 (99.9985%) was purchased from Alfa Aesar. Two step sequential vacuum deposition was adopted for growing $CH_3NH_3PbI_3$. First, PbI_2 layer was deposited on substrates by thermal evaporation at a rate of 0.2 Å/s. After the desired thickness of PbI_2 films is attained, the substrates were taken out and placed on a programmable hot plate in an atmosphere-controlled chamber. The substrates were surrounded by MAI powder and then the chamber was vacuumed. For the conversion process, a temperature of 120 °C was set. A series of samples were obtained by controlling the time of conversion. Different conversion times selected were 5, 6, 8, 12, and 15 hour. Different thickness of PbI_2 films were deposited, so that the final thickness of the perovskite films were ~1 µm. PbI_2 films with thickness 600 nm and 500 nm were used for 5 and 6 hour conversion time. For 8, 12, and 15 hour conversion times, 400 nm PbI_2 film was used. For thermal conductivity measurements, the films were deposited on chips purchased from Linseis. For seebeck and other characterizations, films were deposited on normal glass of dimension 25mm x15mm.

PbI_2 and $CH_3NH_3PbI_3$ film thickness were measured using a Tencor profilometer. XRD of the films was obtained using Bruker D8 Advance diffractometer. SEM images were obtained using FEI Nova Nano 630. UV-Vis spectra were acquired using Cary 6000 spectrometer. FTIR spectra were recorded using Thermo Scientific ATR-FTIR spectrometer. PL spectra were obtained using a Horiba spectrometer. All current-voltage characteristics were carried out using Keithley 4200 semiconductor Analyzer in a Lakeshore probe station. Temperature dependent In-plane thermal conductivity was measured under vacuum using the 3-omega Völklein method with a Linseis Thin Film Analyzer. Samples were prepared onto pre-patterned test chips from Linseis. For the electrical conductivity measurements, parallel line-shape Au electrodes were deposited as the top

contact with width and channel length of 2 mm and 250 μm, respectively. For thermal voltage measurements, a homemade set up was used with peltier devices and thermocouples to apply temperature gradient across the sample under N_2 environment and the voltage was recorded using Keithley 6517B electrometer. Two rectangular Au electrodes (width: 8 mm and length: 15 mm) were deposited on perovskite coated glass substrate with a distance of 9 mm for thermal voltage measurements. All measurments and storage are done under N_2 environment and in dark.

3. RESULTS AND DISCUSSION

Sequential vapor deposition (SVD) procedure[30] for growing smooth and uniform $CH_3NH_3PbI_3$ film is described schematically in Figure 1a. Briefly, highly oriented PbI_2 films (Figure S1) were first deposited by thermal evaporation followed by a treatment of MAI vapor (more details in experimental section). MAI vapor diffuses into PbI_2 film, resulting in hybrid $CH_3NH_3PbI_3$ films consisting of inorganic Pb-I octahedra and organic $CH_3NH_3^+$ cations (Figure 1b). In order to achieve MAI deficient and MAI excess $CH_3NH_3PbI_3$ films, PbI_2 films were treated under MAI vapor for different durations (5, 6, 8, 12 and 15 hours). The X-ray diffraction (XRD) patterns for the optimized $CH_3NH_3PbI_3$ films are shown in Figure 1c. The $CH_3NH_3PbI_3$ film obtained after 5 hour MAI vapor treatment exhibits a significant residual PbI_2 diffraction peak at 12.6°. This residual PbI_2 peak disappears for films treated with MAI for 6 hours and more.

The corresponding UV-Vis spectra of $CH_3NH_3PbI_3$ films with different level of MAI treatment is shown in Figure 1d. The 5 hour film shows higher absorption at lower wavelength region due to presence of residual PbI_2 which has a band edge around 520 nm (Figure S2). Fourier transform infrared (FTIR) spectra exhibits increasing peak strength for the N-H symmetric and asymmetric stretch vibrations with increasing duration of MAI treatment (Figure S3), confirming the presence of different concentration of $CH_3NH_3^+$.[29] Integrating the peak area

for N-H vibration can give an idea on relative concentration of MAI in the films. The 15 hour treated film was found to have 2.7 times higher MA content than the 5 hour (MAI deficient) one (Figure S4). Photoluminescence (PL) measurements exhibited a single peak centered on the energy close to the bandgap and the difference between the intensities for different films was up to half order (Figure S5).

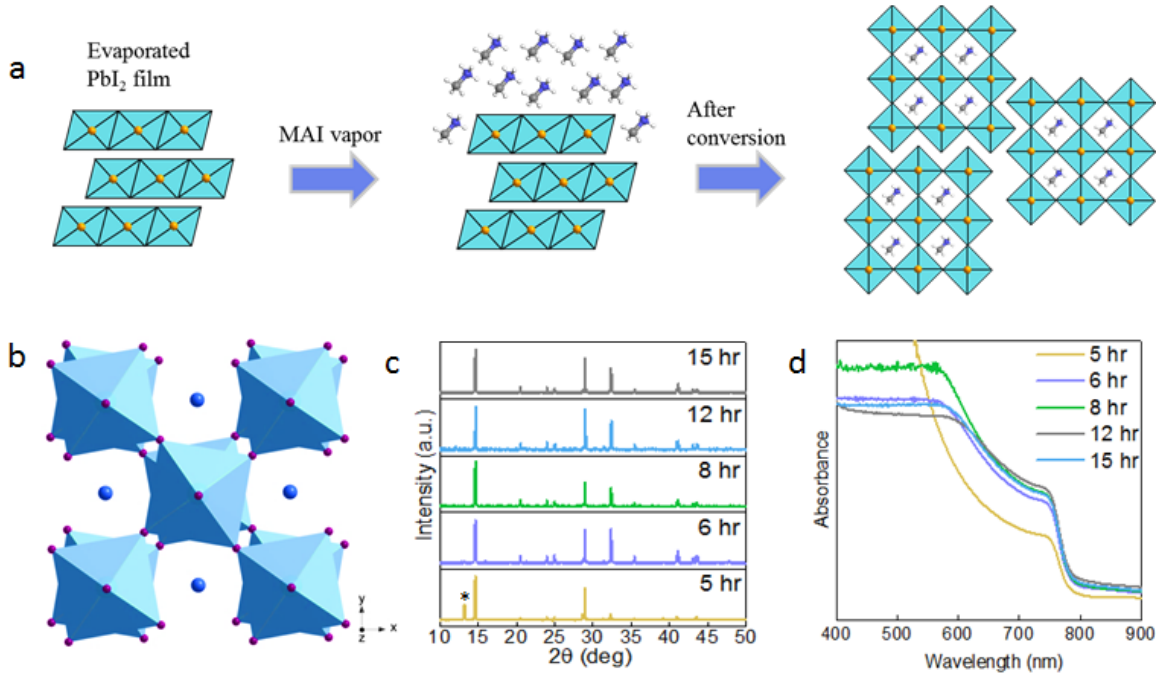

Figure 1. (a) Schematic representation of sequential vapor deposition of perovskite films. (b) Perovskite crystal structure consisting of inorganic Pb-I octahedra and organic $CH_3NH_3^+$ cations (blue spheres). (c) XRD spectra of perovskite films with increasing conversion times of PbI_2 under MAI vapor. Asterisk represents PbI_2 peak. (d) Absorption spectra of the corresponding films in c.

Scanning electron microscope (SEM) images show uniform and smooth SVD perovskite films (Figure 2a-e). Despite the same initial quality of evaporated PbI_2 film (Figure S1), the resulting perovskite films exhibit some degree of deviation in terms of grain morphology for different levels of MAI treatment. The average grain size increases from 0.4 μm (5 hour film) to 1 μm (8 hour) and then it decreases to 0.6 μm for films with 12 and 15 hour MAI treatment

durations. In addition, 12 and 15 hour films show noticeable pin holes at the grain boundaries. To elucidate the effect of different levels of MAI treatment on the electrical behavior of $CH_3NH_3PbI_3$ films, we measured the electrical conductivity which monotonically increased with increasing MAI treatment duration (Figure 2f). Despite the pinholes, this enhancement in conductivity can be attributed to formation of highly conducting pathways (MAI channels) along the grain boundaries.[31]

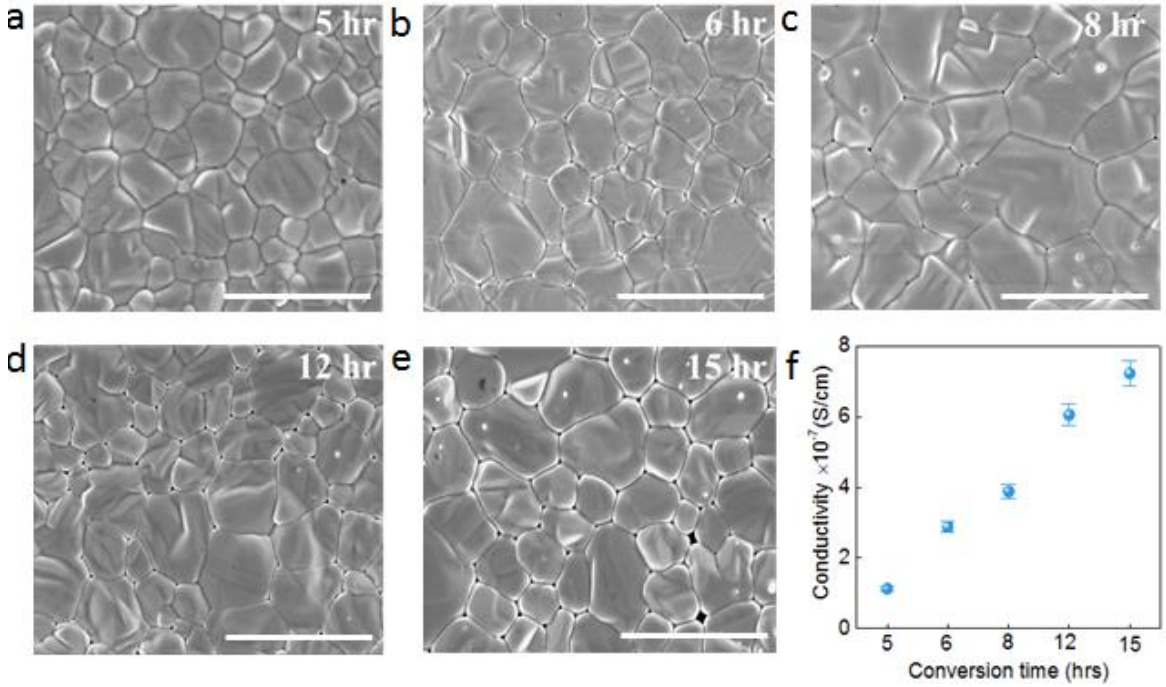

Figure 2. (a-e) SEM images of SVD perovskite films with different conversion times under MAI vapor. Scale bars represent 2 μm. (f) Electrical conductivity evolutions of perovskite films with different conversion times.

Thermal conductivity (κ) and thermopower (S) are two key parameters which provide crucial information about a material system for their applicability in thermoelectrics or for thermal management applications.[32] Most of the prior studies on thermal conductivity of perovskites are accomplished using single crystals with limited information on films.[23] The in-plane thermal conductivity of the vapor deposited perovskite films were measured using a chip-based

3ω method for the first time. Perovskite films (thickness ~1 μm) were grown on pre-patterned chips with different levels of MAI treatment similar to glass substrates as discussed in previous section.

Figure 3a shows the thermal conductivity measured in the temperature range 293-373 K. Interestingly, the thermal conductivity value does not deviate much between different films, exhibiting an ultralow value of 0.32 ± 0.03 W/mK at 293 K. This value is consistent with previous reports measured by different techniques (Table S1). For comparison, we measured the thermal conductivity of PbI_2 film with the same thickness, resulting in a value of 0.22 W/mK at 293 K. Different levels of MAI in perovskite films have a negligible effect on the thermal conductivity of $CH_3NH_3PbI_3$ suggesting it is mainly governed by the Pb-I lattice at room temperature. The effect of $CH_3NH_3^+$ on the thermal conductivity may become pronounced at low temperatures.[33] Furthermore, ultralow thermal conductivity was also observed previously for $CsPbX_3$ (X: halogen) inorganic perovskites which suggests the dominant role of Pb-X cage in determining the thermal conductivity in these compounds at room temperature.[34,35] Such ultralow thermal conductivity can originate from different scattering processes like phonon-impurity, phonon-carrier, phonon-grain boundaries and phonon-phonon. In case of $CH_3NH_3PbI_3$, it is a consensus that the ultralow thermal conductivity at room temperature is due to Umklapp phonon-phonon scattering dictated by the inorganic Pb-I cage.[21,33] In the present work, there was no change in the thermal conductivity around the tetragonal to cubic phase transition. $CH_3NH_3PbI_3$ has two temperature induced phase transitions, orthorhombic to tetragonal around 165 K and tetragonal to cubic around 327 K.[36] In some cases, an abrupt change (dip or jump) in the thermal conductivity around the phase transition temperatures are observed and in other cases it is

not.[17,18,34,37] Also, the degree of this abrupt change is not similar in different reports. This may be attributed to the diverse quality of samples prepared in different studies.

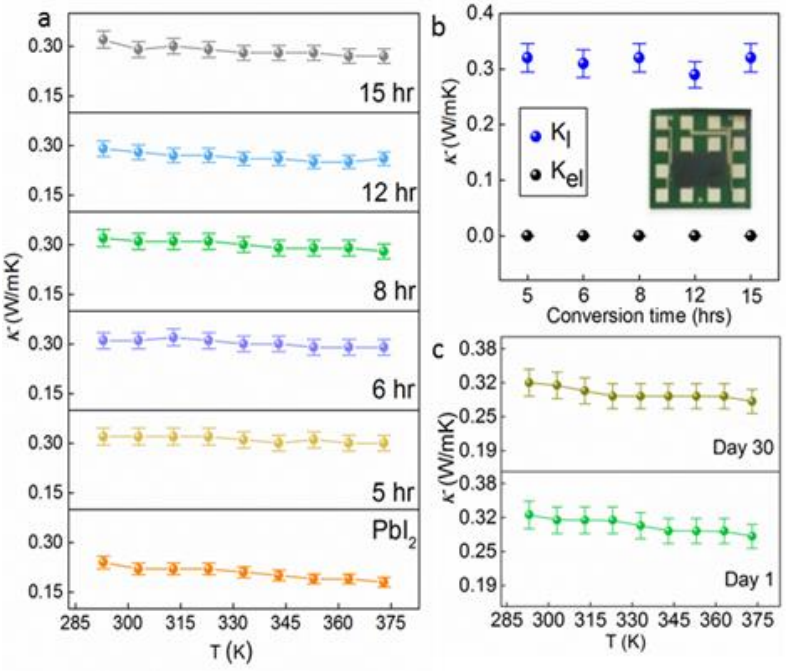

Figure 3. (a) Thermal conductivity of perovskite films with increasing conversion times under MAI vapor and PbI_2 film. (b) Electronic and lattice contributions to the total thermal conductivity at 293 K. Inset shows the perovskite film deposited on the prepatterned chip for thermal conductivity measurements. (c) Comparision of thermal conductivity of the fresh 8 hour MAI treated perovskite film and after 30 days.

The total thermal conductivity can be expressed as $\kappa = \kappa_{el} + \kappa_L$, where κ_{el} and κ_L are contributions from carriers and phonons, respectively. For low conducting materials such as $CH_3NH_3PbI_3$, the electronic contribution is negligible and the dominant contribution comes from the phonons.[17] For the present case, κ_{el} was estimated from the Wiedemann-Franz law, $\kappa_{el} = L\sigma T$, where L_0 is the Lorenz factor and σ is the electrical conductivity of the sample. The phononic contribution (κ_L) which is obtained by subtracting the electrical contribution (κ_{el}) from κ, contributes more than 99% of the total thermal conductivity (Figure 3b). To monitor the stability of the perovskite film, we measured the thermal conductivity of the 8 hour MAI treated film after

dark storage of one month. There was negligible change in the thermal conductivity over the whole temperature range underscoring the excellent stability of the SVD perovskite films.

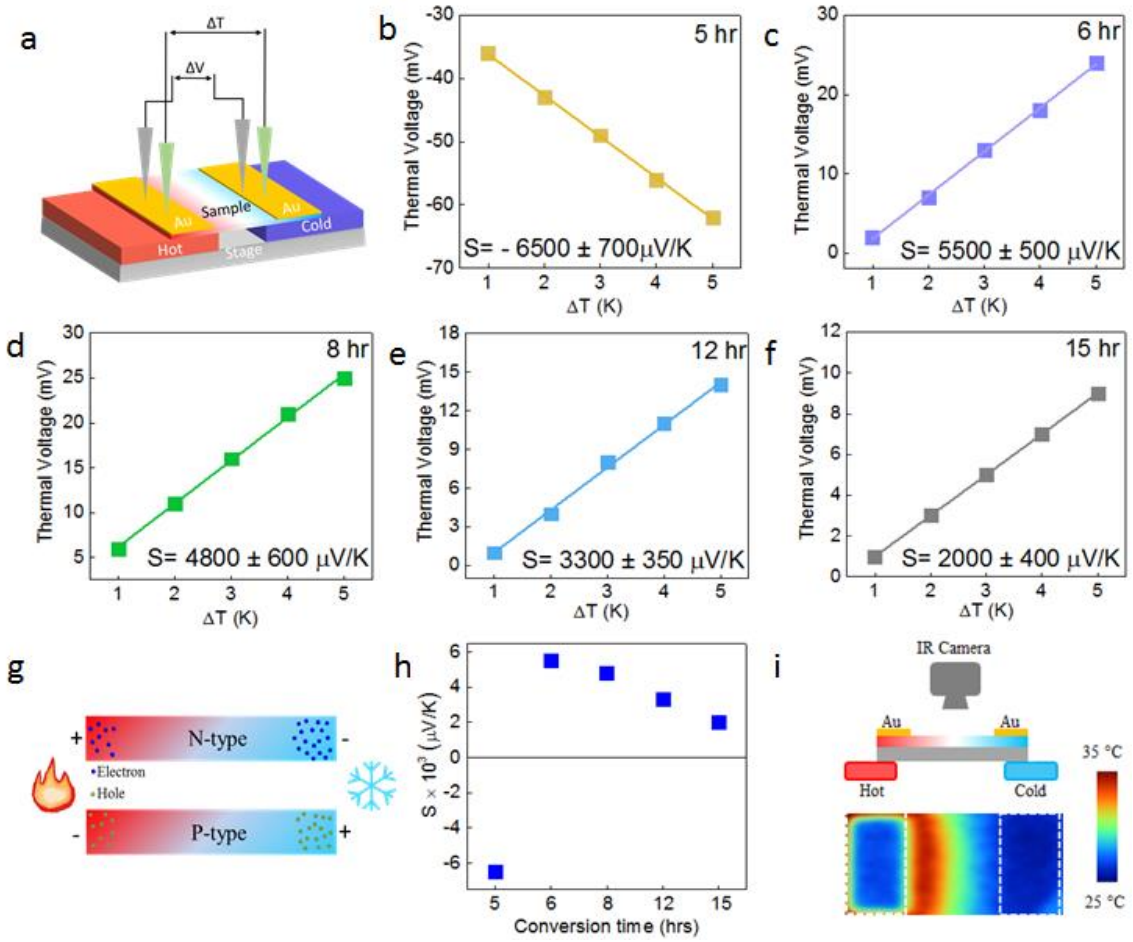

Figure 4. (a) Schematic of the thermopower measurement set up. (b-f) Thermopower of perovskite films with different conversion times under MAI vapor. The straight lines are fitting to the data points. **g)** Carrier transport in *n* and *p* type materials under thermal gradient. (h) Comparison of thermopower (*S*) for different films. (i) An example IR image taken showing the thermal gradient in the sample. Dotted areas indicate the Au contacts. The contacts appear cold in the IR image because of their different emissivity compared to perovskite film.

To examine the effect of composition of $CH_3NH_3PbI_3$ films on the charge carrier type (*p*- or *n*-type), we measured the thermal voltage to deduce the nature of the thermopower. The schematic of the measurement set up is shown in Figure 4a (more details in experimental section). Negative thermopower was recorded for the perovskite films treated for 5 hours under MAI vapor demonstrating it is n-type. It should be noted that this film contains excess PbI_2

(Figure 1c). For the rest of the films (6, 8, 12, 15 hour), we observed positive thermopower indicating their p-type nature (Figure 4b-f). High thermopower were recorded for both *n*- and *p*-type films on the same order that of previously reported perovskite single crystals (Table S2) as a result of extremely low carrier densities.[23] For *p*-type films, the thermopower decreased with increasing level of MAI treatment which can be attributed to correspondingly enhanced conductivity. Electrons and holes are the majority carriers for *n*- and *p*-type films, respectively. For *n*-type films, electrons move from the hot side to the cold side while in case of *p*-type films, holes move towards cold side (Figure 4g).

The origin of *n* and *p* self-doping of $CH_3NH_3PbI_3$ with composition variation can be explained on the basis of defects generated during the growth (Figure S6). For PbI_2 rich (MAI deficient) films, the possible defects are Pb interstitial, MA vacancy and I vacancy. In case of MAI rich (PbI_2 deficient), the defects can be Pb vacancy, MA interstitial and I vacancy. The *n* doping originates from I vacancy in PbI_2 rich films while *p* doping originates from Pb vacancy for MAI rich films due to high formation energies of the other defects in each case.[24,38] In a recent work[39], band edges with respect to fermi level of $CH_3NH_3PbI_3$ were directly measured using scanning tunneling spectroscopy resulting in a transition of electronic conductivity from *p*-type to *n*-type depending on the composition, consistent with present work. The transition (Figure 4h) of thermopower from *n*- to *p*-type in $CH_3NH_3PbI_3$ offers the possibility of fabricating efficient thermoelectrics in the future if the electrical conductivity can be enhanced by suitable strategies such as doping or forming composites. To visualize the temperature gradient of the film, we took an example infrared (IR) image of the film for a temperature difference of 10 K, clearly showing the well-defined temperature distribution. To check the performance stability of

the SVD films, we measured their thermopower after one month of storage in nitrogen. Both *n*- and *p*-type films exhibited steady performance even after four weeks of storage (Figure S7).

4. CONCLUSIONS

In summary, for the first time thermal conductivity and thermopower measurements of vapor deposited $CH_3NH_3PbI_3$ films were accomplished. *n*- and *p*-type $CH_3NH_3PbI_3$ films were achieved by tuning the organic and inorganic precursor compositions. A strong correlation between the organic cation concentration in $CH_3NH_3PbI_3$ film and morphology as well as electrical conductivity was observed. An ultralow in-plane thermal conductivity of 0.32 W/mK at room temperature was recorded for $CH_3NH_3PbI_3$, dominated by the Pb-I inorganic lattice. In addition, high negative and positive thermopower were recorded with good stability under inert atmosphere. The present work provides crucial insights for future hybrid perovskite based thermoelectrics and their thermal management.

ASSOCIATED CONTENT

Supporting Information: PbI_2 layer characterization, PL and FTIR spectra, Stability results.

AUTHOR INFORMATION

Corresponding Author
*E-mail: derya.baran@kaust.edu.sa

Notes
The authors declare no competing financial interest.

ACKNOWLEDGMENT

This publication is based upon work supported by the King Abdullah University of Science and Technology (KAUST) Office of Sponsored Research (OSR) under Award No. OSR-CRG2018-3737.

REFERENCES

(1) Gratzel, M. The light and shade of perovskite solar cells. *Nat. Mater.* **2014,** *13*, 838-842.
(2) Green, M. A.; Ho-Baillie, A.; Snaith, H. J. The emergence of perovskite solar cells. *Nat. Photonics* **2014,** *8*, 506-514.
(3) Jeon, N. J.; Noh, J. H.; Yang, W. S.; Kim, Y. C.; Ryu, S.; Seo, J.; Seok, S. I. Compositional engineering of perovskite materials for high-performance solar cells. *Nature* **2015,** *517*, 476-480.
(4) Park, N.-G.; Grätzel, M.; Miyasaka, T.; Zhu, K.; Emery, K. Towards stable and commercially available perovskite solar cells. *Nat. Energy* **2016,** *1*, 16152.
(5) Green, M. A.; Ho-Baillie, A. Perovskite solar cells: the birth of a new era in photovoltaics. *ACS Energy Lett.* **2017,** *2*, 822-830.
(6) Saidaminov, M. I.; Haque, M. A.; Savoie, M.; Abdelhady, A. L.; Cho, N.; Dursun, I.; Buttner, U.; Alarousu, E.; Wu, T.; Bakr, O. M. Perovskite photodetectors operating in both narrowband and broadband regimes. *Adv. Mater.* **2016,** *28*, 8144-8149.
(7) Zhu, H.; Fu, Y.; Meng, F.; Wu, X.; Gong, Z.; Ding, Q.; Gustafsson, M. V.; Trinh, M. T.; Jin, S.; Zhu, X. Y. Lead halide perovskite nanowire lasers with low lasing thresholds and high quality factors. *Nat. Mater.* **2015,** *14*, 636-642.
(8) Kim, Y.-H.; Cho, H.; Heo, J. H.; Kim, T.-S.; Myoung, N.; Lee, C.-L.; Im, S. H.; Lee, T.-W. Multicolored organic/inorganic hybrid perovskite light-emitting diodes. *Adv. Mater.* **2015,** *27*, 1248-1254.
(9) Guan, X.; Hu, W.; Haque, M. A.; Wei, N.; Liu, Z.; Chen, A.; Wu, T. Light-responsive ion-redistribution-induced resistive switching in hybrid perovskite schottky junctions. *Adv. Funct. Mater.* **2018,** *28*, 1704665.
(10) Lee, M. M.; Teuscher, J.; Miyasaka, T.; Murakami, T. N.; Snaith, H. J. Efficient hybrid solar cells based on meso-superstructured organometal halide perovskites. *Science* **2012,** *338*, 643-647.
(11) Xing, G.; Mathews, N.; Sun, S.; Lim, S. S.; Lam, Y. M.; Gratzel, M.; Mhaisalkar, S.; Sum, T. C. Long-range balanced electron- and hole-transport lengths in organic-inorganic $CH_3NH_3PbI_3$. *Science* **2013,** *342*, 344-347.
(12) Stranks, S. D.; Nayak, P. K.; Zhang, W.; Stergiopoulos, T.; Snaith, H. J. Formation of thin films of organic–inorganic perovskites for high-efficiency solar cells. *Angew. Chem. Int. Ed.* **2015,** *54*, 3240-3248.
(13) Zhumekenov, A. A.; Burlakov, V. M.; Saidaminov, M. I.; Alofi, A.; Haque, M. A.; Turedi, B.; Davaasuren, B.; Dursun, I.; Cho, N.; El-Zohry, A. M.; et al. The role of surface tension in the crystallization of metal halide perovskites. *ACS Energy Lett.* **2017,** *2*, 1782-1788.
(14) Kazim, S.; Nazeeruddin, M. K.; Grätzel, M.; Ahmad, S. Perovskite as light harvester: a game changer in photovoltaics. *Angew. Chem. Int. Ed.* **2014,** *53*, 2812-2824.
(15) Saliba, M.; Correa-Baena, J.-P.; Grätzel, M.; Hagfeldt, A.; Abate, A. Perovskite solar cells: from the atomic level to film quality and device performance. *Angew. Chem. Int. Ed.* **2018,** *57*, 2554-2569.
(16) Zhumekenov, A. A.; Saidaminov, M. I.; Haque, M. A.; Alarousu, E.; Sarmah, S. P.; Murali, B.; Dursun, I.; Miao, X.-H.; Abdelhady, A. L.; Wu, T.; et al. Formamidinium lead halide perovskite crystals with unprecedented long carrier dynamics and diffusion length. *ACS Energy Lett.* **2016,** *1*, 32-37.

(17) Pisoni, A.; Jacimovic, J.; Barisic, O. S.; Spina, M.; Gaal, R.; Forro, L.; Horvath, E. Ultra-low thermal conductivity in organic-inorganic hybrid perovskite $CH_3NH_3PbI_3$. *J. Phys. Chem. Lett.* **2014,** *5*, 2488-2492.
(18) Ye, T.; Wang, X. Z.; Li, X. Q.; Yan, A. Q.; Ramakrishna, S.; Xu, J. W. Ultra-high Seebeck coefficient and low thermal conductivity of a centimeter-sized perovskite single crystal acquired by a modified fast growth method. *J. Mater. Chem. C* **2017,** *5*, 1255-1260.
(19) Heiderhoff, R.; Haeger, T.; Pourdavoud, N.; Hu, T.; Al-Khafaji, M.; Mayer, A.; Chen, Y. W.; Scheer, H. C.; Riedl, T. Thermal conductivity of methylammonium lead halide perovskite single crystals and thin films: a comparative study. *J. Phys. Chem. C* **2017,** *121*, 28306-28311.
(20) Elbaz, G. A.; Ong, W. L.; Doud, E. A.; Kim, P.; Paley, D. W.; Roy, X.; Malen, J. A. Phonon speed, not scattering, differentiates thermal transport in lead halide perovskites. *Nano Lett.* **2017,** *17*, 5734-5739.
(21) Wang, M.; Lin, S. Anisotropic and ultralow phonon thermal transport in organic-inorganic hybrid perovskites: atomistic insights into solar cell thermal management and thermoelectric energy conversion efficiency. *Adv. Funct. Mater.* **2016,** *26*, 5297-5306.
(22) Stoumpos, C. C.; Malliakas, C. D.; Kanatzidis, M. G. Semiconducting tin and lead iodide perovskites with organic cations: phase transitions, high mobilities, and near-infrared photoluminescent properties. *Inorg. Chem.* **2013,** *52*, 9019-9038.
(23) Wu, T.; Mukherjee, R.; Ovchinnikova, O. S.; Collins, L.; Ahmadi, M.; Lu, W.; Kang, N. G.; Mays, J. W.; Jesse, S.; Mandrus, D.; et al. Metal/ion interactions induced p-i-n junction in methylammonium lead triiodide perovskite single crystals. *J. Am. Chem. Soc.* **2017,** *139*, 17285-17288.
(24) Wang, Q.; Shao, Y.; Xie, H.; Lyu, L.; Liu, X.; Gao, Y.; Huang, J. Qualifying composition dependent p and n self-doping in $CH_3NH_3PbI_3$. *Appl. Phys. Lett.* **2014,** *105*, 163508.
(25) Kim, J.; Lee, S. H.; Lee, J. H.; Hong, K. H. The role of intrinsic defects in methylammonium lead iodide perovskite. *J. Phys. Chem. Lett.* **2014,** *5*, 1312-1317.
(26) Jacobsson, T. J.; Correa-Baena, J.-P.; Halvani Anaraki, E.; Philippe, B.; Stranks, S. D.; Bouduban, M. E. F.; Tress, W.; Schenk, K.; Teuscher, J.; Moser, J.-E.; et al. Unreacted PbI_2 as a double-edged sword for enhancing the performance of perovskite solar cells. *J. Am. Chem. Soc.* **2016,** *138*, 10331-10343.
(27) Park, B. W.; Kedem, N.; Kulbak, M.; Lee, D. Y.; Yang, W. S.; Jeon, N. J.; Seo, J.; Kim, G.; Kim, K. J.; Shin, T. J.; et al. Understanding how excess lead iodide precursor improves halide perovskite solar cell performance. *Nat. Commun.* **2018,** *9*, 3301.
(28) Cui, P.; Wei, D.; Ji, J.; Huang, H.; Jia, E.; Dou, S.; Wang, T.; Wang, W.; Li, M. Planar p–n homojunction perovskite solar cells with efficiency exceeding 21.3%. *Nat. Energy* **2019,** *4*, 150-159.
(29) Dänekamp, B.; Müller, C.; Sendner, M.; Boix, P. P.; Sessolo, M.; Lovrincic, R.; Bolink, H. J. Perovskite–perovskite homojunctions via compositional doping. *J. Phys. Chem. Lett.* **2018,** *9*, 2770-2775.
(30) Chen, C. W.; Kang, H. W.; Hsiao, S. Y.; Yang, P. F.; Chiang, K. M.; Lin, H. W. Efficient and uniform planar-type perovskite solar cells by simple sequential vacuum deposition. *Adv. Mater.* **2014,** *26*, 6647-6652.
(31) Son, D.-Y.; Lee, J.-W.; Choi, Y. J.; Jang, I.-H.; Lee, S.; Yoo, P. J.; Shin, H.; Ahn, N.; Choi, M.; Kim, D.; et al. Self-formed grain boundary healing layer for highly efficient $CH_3NH_3PbI_3$ perovskite solar cells. *Nat. Energy* **2016,** *1*, 16081.

(32) Sootsman, J. R.; Chung, D. Y.; Kanatzidis, M. G. New and old concepts in thermoelectric materials. *Angew. Chem. Int. Ed.* **2009,** *48*, 8616-8639.
(33) Kovalsky, A.; Wang, L.; Marek, G. T.; Burda, C.; Dyck, J. S. Thermal conductivity of $CH_3NH_3PbI_3$ and $CsPbI_3$: measuring the effect of the methylammonium ion on phonon scattering. *J. Phys. Chem. C* **2017,** *121*, 3228-3233.
(34) Ge, C.; Hu, M.; Wu, P.; Tan, Q.; Chen, Z.; Wang, Y.; Shi, J.; Feng, J. Ultralow thermal conductivity and ultrahigh thermal expansion of single-crystal organic–inorganic hybrid perovskite $CH_3NH_3PbX_3$ (X = Cl, Br, I). *J. Phys. Chem. C* **2018,** *122*, 15973-15978.
(35) Caddeo, C.; Melis, C.; Saba, M. I.; Filippetti, A.; Colombo, L.; Mattoni, A. Tuning the thermal conductivity of methylammonium lead halide by the molecular substructure. *Phys. Chem. Chem. Phys.* **2016,** *18*, 24318-24324.
(36) Deretzis, I.; La Magna, A. Exploring the orthorhombic-tetragonal phase transition in $CH_3NH_3PbI_3$: the role of atom kinetics. *Nanoscale* **2017,** *9*, 5896-5903.
(37) Guo, Z.; Yoon, S. J.; Manser, J. S.; Kamat, P. V.; Luo, T. Structural phase- and degradation-dependent thermal conductivity of $CH_3NH_3PbI_3$ perovskite thin films. *J. Phys. Chem. C* **2016,** *120*, 6394-6401.
(38) Yin, W.-J.; Shi, T.; Yan, Y. Unusual defect physics in $CH_3NH_3PbI_3$ perovskite solar cell absorber. *Appl. Phys. Lett.* **2014,** *104*, 063903.
(39) Paul, G.; Chatterjee, S.; Bhunia, H.; Pal, A. J. Self-doping in hybrid halide perovskites via precursor stoichiometry: to probe the type of conductivity through scanning tunneling spectroscopy. *J. Phys. Chem. C* **2018,** *122*, 20194-20199.

TOC Graphic

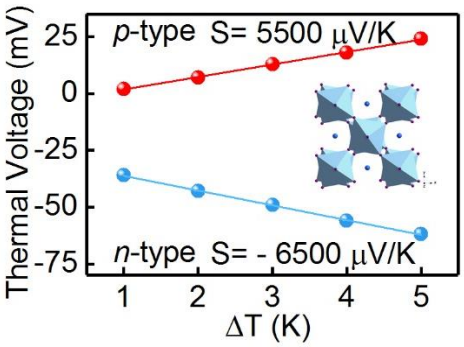
p-type S= 5500 μV/K
n-type S= - 6500 μV/K
Thermal Voltage (mV)
25
0
-25
-50
-75
1
2
3
4
5
ΔT (K)